Supporting Information

Russo and Golovchenko 10.1073/pnas.1119827109

SI Text

Additional Electron Microscopy. *Selected area diffraction.* Fig. S1 contains a selected area electron diffractogram from the graphene region encompassing the pore in Fig. 2 and Movie S1, taken with the beam perpendicular to the plane of the lattice. Arrowheads point to the (110) Bragg reflection (1.23 Å spacing) and to the (210) reflection (2.13 Å spacing), which are of approximately equal intensity, confirming the graphene is a single atomic layer thick. Similar diffractograms were collected for each region of interest to verify that they were monolayer graphene. Nominal instrument camera length was 450 mm.

Electron exit wave reconstruction. During the continuous exposure of the pore in Fig. 2, a defocus image series of 12 images at 10 Å defocus steps was collected. We used these data to reconstruct the electron exit wave function using the MacTempas software package. The phase of the reconstructed wave is presented in Fig. S2 with the phase image rendered at +270 Å focus, and convolved with a Gaussian blurring function of 0.3 Å FWHM.

Additional pore trajectories. In addition to the pore presented in Fig. 3, four additional pores were analyzed using the same method, and all five trajectories are presented in Fig. S3 using a different color and data point symbol for each. These are the same pores presented in Movie S2. Theoretically, the distribution of the y-axis intercepts of the radius vs. dose trajectories should directly reflect the initial distribution of nucleation defect types. And because the initial number of edge atoms is a small integer value (3–4 edge atoms for a 1–2 atom defect in a hexagonal lattice, neglecting reconstruction effects), the relative variance in the number of edge atoms at the beginning of pore formation is large and thus the variance in initial radius is large. The surface contaminant molecules may also play a role at the beginning of pore growth as they may temporarily bind to dangling bonds in a defect site and influence the removal of the first few atoms of the growth trajectory. We expect this mechanism accounts for most of the variation in the y-intercepts of the five linear fits in Fig. S3, whose value is -0.1 ± 2.7 Å. The influence of contaminant molecules should decrease as the edge of the pore increases, which is what we observe in the experiments because the slope becomes very reproducible after the radius increases to just a few angstroms. More measurements on samples with less surface contaminants will improve the accuracy of the intercepts, and might allow one to distinguish the specific type of defect that nucleated a given pore growth trajectory.

Control experiment with no ion irradiation. Fig. S4 shows an electron micrograph of a suspended graphene monolayer treated identically to that in Fig. 4 except with no ion irradiation. No pores are visible in the 1.96×10^6 Å^2 area of the image. The image was low pass filtered to 1.0 Å and adjusted to eight bits of linear contrast spanning approximately 2σ about the mean value.

Cross-section and Bond Energy Calculations. The total cross-section σ_d for a collision of a high energy electron with a bound atom, where the energy transferred is sufficient to remove the atom, was calculated by Seitz and Koehler (1), and is given by

$$\sigma_d = \left(\frac{Zq_e^2}{\epsilon_0 2m_0 c^2}\right)^2 \left(\frac{1-\beta^2}{4\pi\beta^4}\right) \left\{ \frac{T_m}{E_d} - 1 - \beta^2 \ln\left(\frac{T_m}{E_d}\right) \right.$$
$$\left. + \frac{\pi Zq_e^2 \beta}{\hbar c}\left[2\sqrt{\frac{T_m}{E_d}} - \ln\left(\frac{T_m}{E_d}\right) - 2\right]\right\}, \qquad \textbf{[S1]}$$

where q_e is the electron charge, m_0 is the electron rest mass, Z is the atomic number, $\hbar$ is the reduced Planck constant, c is the speed of light, $\beta = v/c$ where v is the electron velocity, ϵ_0 is the permittivity of free space, and E_d is the energy required to displace an atom from the molecule. T_m, the maximum transmitted energy in a single scattering event, occurs with a direct head on collision; in the relativistic formulation this energy is given by

$$T_m = \frac{2ME(E + 2m_0 c^2)}{(M + m_0)^2 c^2 + 2ME}, \qquad \textbf{[S2]}$$

where E is the incident electron energy and M is the mass of the atom. This expression for total cross-section is plotted for the region of interest in Fig. S5 for 80 keV electrons ($T_m = 15.66$ eV) colliding with carbon atoms.

Because Eq. **S1** is a transcendental equation, we numerically determined the values of E_d from our measured values of σ_d, and the results for the five pores in Fig. S4 are plotted as black circles. The red dot is the mean value of $\sigma_d = 8.9 \times 10^{-24}$ cm^2, which corresponds to 14.1 eV. The plot also shows the error analysis for the average cross-section and displacement energy, where the black error bar indicates the random error in the measurement ($\pm 1\sigma$) and red error bar indicates the estimated systemic error, as propagated through the calculations, whose largest component is the beam current measurement. Because the potential error in the beam current measurement is due to the loss of backscattered and secondary electrons from the Faraday cup (<20% of the beam current), the systematic error bound is larger in one direction.

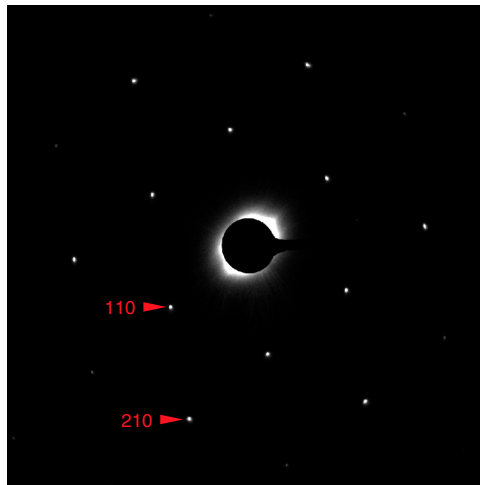1. Seitz F, Koehler JS (1956) Displacement of atoms during irradiation. *Solid State Phys* 2:305–448.

Fig. S1. Electron diffraction micrograph of single layer graphene region encompassing the pore in Fig. 2 and Movie S1.
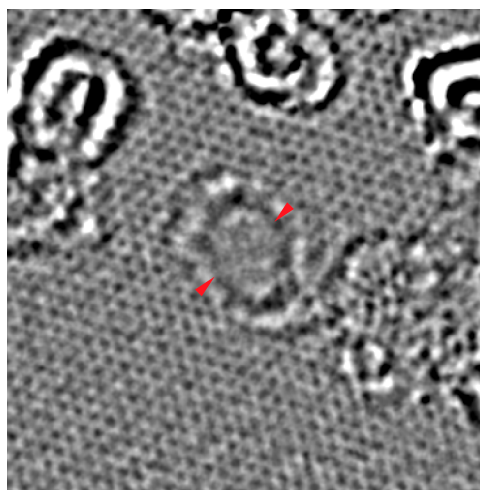

Fig. S2. Electron exit wave phase reconstruction image of pore in Fig. 2. Arrowheads span 11 Å, and image is 70 × 70 Å.
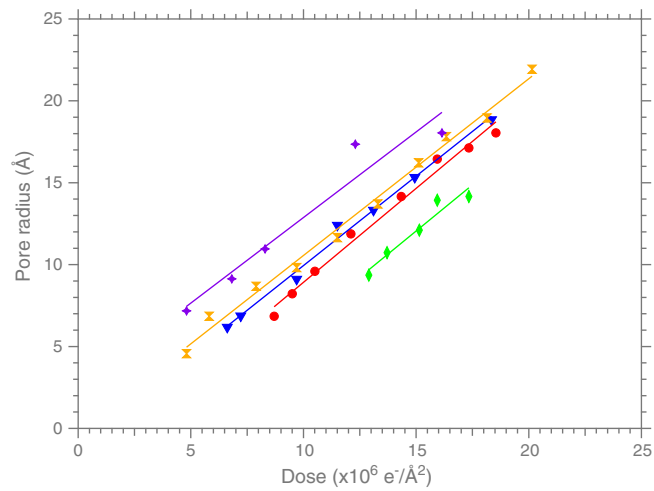

Fig. S3. Radius vs. dose trajectory plots of five pores.

Fig. S4. Electron micrograph of graphene with no ion irradiation. Image taken after electron dose of 9.7×10^6 e$^-$/Å^2 for comparison with Fig. 4.

Fig. S5. Plot of total cross-section (σ_d) vs. displacement energy (E_d) at 80 keV.

Movie S1. Time-lapse micrograph series of the opening of the nanopore shown in Fig. 2. Images are at 30 s intervals with several gaps during which the focus and alignments of the electron microscope were readjusted. We also note that there is a defect structure near the growing pore visible in the lower right corner of the movie and these and the nearby contaminant molecules may have influenced the circular symmetry of this pore's growth, but the overall effect is minor relative to the edge-atom removal mechanism. All images were low-pass filtered with a 1.0 Å cutoff, cropped to 70 × 70 Å, adjusted for brightness and contrast on a linear scale of eight-bit depth, combined into one image stack and compressed with MPEG-4 compression to create a 20 frame per second quick time movie file.

Movie S1 (MOV)
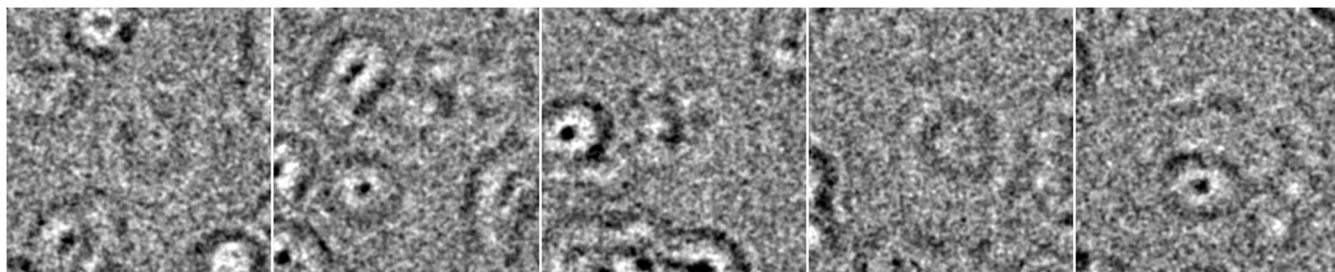
Movie S2. Time-lapse micrograph series of the opening of five additional nanopores, all from the same sample. Images are at 60 s intervals, again with several gaps during which the focus and alignments of the electron microscope were readjusted. All the pores have the same cumulative dose in a given image frame. Image processing was the same as for Movie S1.

Movie S2 (MOV)